

An overview of quasinormal modes in modified and extended gravity

Flora Moulin,¹ Aurélien Barrau,¹ and Killian Martineau¹

¹*Laboratoire de Physique Subatomique et de Cosmologie, Université Grenoble-Alpes, CNRS/IN2P3
53, avenue des Martyrs, 38026 Grenoble cedex, France*

As gravitational waves are now being nearly routinely measured with interferometers, the question of using them to probe new physics becomes increasingly legitimate. In this article, we rely on a well established framework to investigate how the complex frequencies of quasinormal modes are affected by different models. The tendencies are explicitly shown, for both the pulsation and the damping rate. This opportunity is also taken to derive the Regge-Wheeler equation for general static and spherically symmetric metrics.

INTRODUCTION

General relativity (GR) is our best theory of space-time. Although the Lovelock theorem ensures that it cannot be easily modified there are quite a lot of attempts to relax some hypotheses and build a deepest model to describe the gravitational field. From effective quantum gravity to improved infrared properties, the motivations to go beyond GR are countless. So are the situations, both in astrophysics and cosmology, where extended gravity theories can, in principle be tested. In practice, reaching the level of accuracy useful to probe the relevant range of parameters is obviously far from trivial. In this article we focus on a specific aspect of gravitational waves that would be emitted during the relaxation phase of a deformed black hole (BH).

We will consider quasinormal modes associated with the ringdown phase of a BH merging. The modes are not strictly normal due to energy losses of the system through gravitational waves. The boundary conditions for the equation of motion are unusual as the wave has to be purely outgoing at infinity and purely ingoing at the event horizon. The radial part reads as (an introductory review can be found in [1])

$$e^{-i\omega t} = e^{-i(\omega_R + i\omega_I)t}, \quad (1)$$

the complex pulsation ω being split in a real part ω_R , which corresponds to the frequency, and an imaginary one ω_I , which is the inverse timescale of the damping. Stability requires $\omega_I < 0$. Although real-life BHs are spinning, we focus on Schwarzschild solutions in this article. The details of the predictions can therefore not be used to be directly confronted with observations. We however expect the general tendencies and orders of magnitudes to remain correct.

The metric can be submitted to “axial” and “polar” perturbations. In GR, they are described by different equations. The (so called Regge-Wheeler) potential for

axial perturbations is

$$V_\ell^{\text{RG}}(r) = \left(1 - \frac{2M}{r}\right) \left[\frac{\ell(\ell+1)}{r^2} - \frac{6M}{r^3} \right], \quad (2)$$

while the (so-called Zerilli) one for polar perturbations is

$$V_\ell^{\text{Z}}(r) = \frac{2}{r^3} \left(1 - \frac{2m}{r}\right) \times \frac{9M^3 + 3a^2Mr^2 + a^2(1+a)r^3 + 9M^2ar}{(3M + ar)^2}, \quad (3)$$

where $a = \ell(\ell+1)/2 - 1$. In the purely gravitational sector, one needs $\ell \geq 2$. Interestingly, both those equations have the very same spectrum of quasinormal modes (QNMs). This property, called isospectrality [2] is not always true in modified gravity (see [3] for an extension and a discussion of the original proof). Basically, quasinormal modes are described by their multipole number ℓ and their overtone number n . The fundamental quadrupolar mode ($n = 0$ and $\ell = 2$) for a Schwarzschild BH in GR is given by $M\omega \approx 0.374 - 0.0890i$.

There are many different ways to calculate the QNMs: continued fractions, Frobenius series, Mashhoon method, confluent Heun's equation, characteristic integration, shooting, WKB approximations, etc. In this article we focus on the last approach. For most models considered here, the QNMs have already been calculated in previous studies. However this has most of the time been done for $s = 0$ or $s = 1$, not for $s = 2$ as we have done it here. More importantly, it is in addition very useful to rely on the very same method to investigate all models so that the differences underlined are actually due to physical effects and not to numerical issues. Even when the same approach is considered, the way it is implemented is often different enough, between articles, so that it is hard to really compare the results. This is why we have here tried to consider methodically several modified gravity models with a well controlled WKB approximation scheme used in the same way in all cases so as to compare the tendencies between modified gravity proposals.

The determination of the complex frequencies of QNMs is difficult (see [4, 5] for historical reviews and [6, 7] for results based on numerical approaches). This work is based on the WKB approach described in [8]. Following the pioneering work [9], the WKB method for QNMs was developed in [10–13]. This formalism leads to fairly good approximations, especially for high multipole and low overtone numbers. In the following, we restrict ourselves to $n < l$ and use the 6th order WKB method developed by Konoplya [8] (see also [14]). This allows one to recast the potential appearing in the effective Schrödinger equation felt by gravitational perturbations in a complex but tractable form.

The aim of this introductory paper is to investigate how several modified gravity theories impact the QNMs. There are several ways to go beyond GR: extra dimensions, weak equivalence principle violations, extra fields, diffeomorphism-invariance violations, etc. Beyond those technicalities, there are strong conceptual motivations to go beyond the classical theory, from the building of an effective quantum gravity theory to the improvements of the renormalisation properties, through the implementation of a dynamical cosmological constant.

PERTURBATION DYNAMICS

The QNMs are solutions of a perturbation equation with the specific boundary conditions given in the previous section. The radial and angular part can be separated. The radial part is governed by a Schrödinger-like equation:

$$\frac{d^2 Z}{dr^{*2}} + V(r)Z = 0, \quad (4)$$

where Z is the radial part of the “perturbation” variable, assumed to have a time-dependence $e^{i\sigma t}$, and r^* is the tortoise coordinate. For a metric such that:

$$ds^2 = f(r)dt^2 - f(r)^{-1}dr^2 - r^2 d\theta^2 - r^2 \sin^2 \theta d\phi^2, \quad (5)$$

the tortoise coordinate is defined by

$$dr^* = \frac{1}{f(r)} dr. \quad (6)$$

It tends to $-\infty$ at the event horizon and to $+\infty$ at spatial infinity.

As explained previously, BH gravitational perturbations can be of two different types distinguished by their behavior under a parity transformation. For an angular momentum l , axial perturbations transform as $(-1)^l$

under parity, while polar perturbations transform as $(-1)^{l+1}$. This leads to two different potentials in Eq.(4). The potential for the gravitational axial perturbations reads in full generality for the metric given by Eq. (5):

$$V(r) = f(r) \left(\frac{\lambda + 2(f(r) - 1)}{r^2} - \frac{f'(r)}{r} \right). \quad (7)$$

In this work we will not consider the isospectrality-violation issues and we will focus only on such perturbations. It should anyway be kept in mind that, in principle, isospectrality might not hold.

The boundary conditions can be expressed as

$$\begin{aligned} Z &\sim e^{-i\sigma r^*} & r^* &\rightarrow -\infty, \\ Z &\sim e^{i\sigma r^*} & r^* &\rightarrow +\infty. \end{aligned} \quad (8)$$

We shall now derive the Regge-Wheeler equation for the more general (spherical and static) metric:

$$ds^2 = A(r)dt^2 - B(r)^{-1}dr^2 - H(r)d\theta^2 + H(r)\sin^2\theta d\phi^2. \quad (10)$$

For this metric, the tortoise coordinate is defined by

$$\frac{d}{dr^*} = \sqrt{AB} \frac{d}{dr}. \quad (11)$$

The general form of an axisymmetric metric can be written as :

$$ds^2 = e^{2\nu}(dx^0)^2 - e^{2\psi}(dx^1 - \omega dx^0 - q_2 dx^2 - q_3 dx^3)^2 - e^{2\mu_2}(dx^2)^2 - e^{2\mu_3}(dx^3)^2 \quad (12)$$

where $t = x^0$, $\phi = x^1$, $r = x^2$ and $\theta = x^3$. The metric given by Eq. (10) corresponds to:

$$\begin{aligned} e^{2\nu} &= A(r), & e^{-2\mu_2} &= B(r), \\ e^{2\mu_3} &= H(r), & e^{2\psi} &= H(r)\sin^2\theta, \\ \omega &= q_2 = q_3 = 0. \end{aligned} \quad (13)$$

A perturbation of this kind of spacetime is described by ω , q_2 and q_3 , assumed to be first order quantities, and by infinitesimal increments, $\delta\nu$, $\delta\mu_2$, $\delta\mu_3$, of the other quantities.

The components of the Ricci and Einstein tensors for the line element given by Eq. (12) are given in [2]. As we focus here on the axial perturbations, we are interested in the equations governing ω , q_2 and q_3 . These equations are described by the vanishing of the Ricci tensor components:

$$R_{12} = R_{13} = 0. \quad (14)$$

For Eq. (12), one has

$$R_{12} = \frac{1}{2} e^{-2\Psi - \mu_2 - \mu_3} \times [(e^{-3\psi - \nu - \mu_2 + \mu_3} Q_{02})_{,0} - (e^{-3\psi + \nu - \mu_2 - \mu_3} Q_{32})_{,3}], \quad (15)$$

with

$$Q_{ab} = q_{a,b} - q_{b,a} \quad \text{and} \quad Q_{a0} = q_{a,0} - w_{,a} \quad \text{for} \quad a, b = 2, 3. \quad (16)$$

The component R_{13} is also given by Eq. (15) by switching indices 2 and 3.

After replacing ν , μ_2 , μ_3 and ψ by their expressions, $\delta R_{12} = 0$ leads to

$$(H \sin^3 \theta \sqrt{AB} Q_{23})_{,3} = -H^2 \sin^3 \theta \sqrt{\frac{A}{B}} Q_{02,0}. \quad (17)$$

By defining

$$Q = \sqrt{AB} H Q_{23} \sin^3 \theta, \quad (18)$$

one obtains

$$\sqrt{\frac{A}{B}} \frac{1}{H^2 \sin^3 \theta} \frac{\partial Q}{\partial \theta} = Q_{20,0}. \quad (19)$$

For $\delta R_{13} = 0$, one is led to

$$\frac{\sqrt{AB}}{H \sin^3 \theta} \frac{\partial Q}{\partial r} = -Q_{30,0}. \quad (20)$$

We assume that perturbation have a time dependance given by $e^{i\sigma t}$. This implies that Eqs. (19) and (20) read

$$\sqrt{\frac{A}{B}} \frac{1}{H^2 \sin^3 \theta} \frac{\partial Q}{\partial \theta} = -\sigma^2 q_2 - i\sigma \omega_{,2}, \quad (21)$$

$$\frac{\sqrt{AB}}{H \sin^3 \theta} \frac{\partial Q}{\partial r} = \sigma^2 q_3 + i\sigma \omega_{,3}. \quad (22)$$

Taking the derivative of Eq.(21) with respect to θ , the derivative of Eq. (22) with respect to r , and combining the results leads to:

$$\sin^3 \theta \frac{\partial}{\partial \theta} \left(\frac{1}{\sin^3 \theta} \frac{\partial Q}{\partial \theta} \right) + \frac{H^2 B}{A} \frac{\partial}{\partial r} \left(\frac{\sqrt{AB}}{H} \frac{\partial Q}{\partial r} \right) + \sigma^2 \frac{QH}{A} = 0. \quad (23)$$

As suggested in [2], one can then separate the variables r and θ using

$$Q(r, \theta) = R(r) C_{l+2}^{-3/2}(\theta) \quad (24)$$

with C_n^m the Gegenbauer function satisfying

$$\left(\frac{d}{d\theta} \sin^{2m} \theta \frac{d}{d\theta} + n(n+2m) \sin^{2m} \theta \right) C_n^m(\theta) = 0. \quad (25)$$

Inserting Eq. (24) into Eq. (23), one is led to following radial equation:

$$H^2 \frac{B}{A} \frac{\partial}{\partial r} \left(\frac{\sqrt{AB}}{H} \frac{\partial R(r)}{\partial r} \right) + \frac{H}{A} \sigma^2 \mu^2 R(r) = 0, \quad (26)$$

where $\mu^2 = (l-1)(l+2)$. Defining Z so that $R = \sqrt{H} Z$ and using the tortoise coordinate, we are led to a Schrödinger-like equation:

$$\frac{d^2 Z}{dr^{*2}} + (\sigma^2 - V(r)) Z = 0, \quad (27)$$

where the potential is

$$V(r) = \frac{1}{2H^2} \left(\frac{dH}{dr^*} \right)^2 + \frac{\mu^2 A}{H} - \frac{1}{\sqrt{H}} \frac{d^2}{dr^{*2}} \left(\sqrt{H} \right). \quad (28)$$

The potential effectively tends to Eq. (7) for $A(r) = B(r)$ and $H(r) = r^2$. This derivation is useful to calculate QNMs for general static and spherically symmetric metrics.

THE WKB APPROXIMATION

The WKB approximation [10–12] is known for leading to good approximations (compared to numerical results) for the QNMs. The potential is written using the tortoise coordinate so as to be constant at $r^* \rightarrow 0$ (which represent the horizon of the BH) and at $r^* \rightarrow +\infty$ (which represents spatial infinity). The maximum of the potential is reached at r_0^* . Three regions can be identified: region *I* from $-\infty$ to r_1 , the first turning point (where the potential vanishes), region *II* from r_1 to r_2 , the second turning point, and region *III* from r_2 to $+\infty$. In region *II*, a Taylor expansions is performed around r_0^* . In regions *I* and *III*, the solution is approximated by an exponential function:

$$Z \sim \exp \left[\frac{1}{\epsilon} \sum_{n=0}^{\infty} \epsilon^n S_n(x) \right], \quad \epsilon \rightarrow 0. \quad (29)$$

This expression can be inserted into Eq. (4) so as to obtain S_j as a function of the potential and its derivative.

We then impose the boundary conditions given by Eq. (9) and match the solutions of regions *I* and *III* with the solution for region *II* at the turning points r_1 and r_2 (respectively). The WKB approximation has been usefully extended from the third to sixth order in [8].

This allows one to derive the complex frequencies as a function of the potential and its derivatives evaluated at the maximum. For the sixth order treatment, one is led to:

$$\omega^2 = V_0 - i\sqrt{-2V_0''} \left(\sum_{j=2}^6 \Lambda_j + n + \frac{1}{2} \right), \quad (30)$$

where the expressions of the Λ_j s can be found in [8]. In the following, we use this scheme to compare different modified gravity models and we present results only in the range of validity of the WKB approximations.

MODIFIED GRAVITY MODELS AND RESULTS

Throughout all this section we investigate some properties of the QNMs for several extended gravity approaches. We pretend, in no way, to do justice to the subtleties of those models and, when necessary, we explicitly choose a specific of simplified setting to make the calculations easily tractable.

As we focus on phenomenological aspects, the more interesting mode is the fundamental one: $n = 0$ and $l = 2$. We therefore focus on a few points around this one (keeping in mind that the accuracy is better for higher values of l). In all the figures, the lower overtone n is the one with the smallest imaginary part.

We first consider models with a metric of the form:

$$ds^2 = f(r)dt^2 - f(r)^{-1}dr^2 - r^2d\theta^2 - r^2\sin^2\theta d\phi^2, \quad (31)$$

and, then, investigate a model with two different metric functions, using the result obtained in Eq. (28).

1. Massive gravity

In GR, the graviton is a massless spin-2 particle. One of the first motivations for modern massive gravity – which can be seen as a generalization of GR – was the hope to account for the accelerated expansion of the Universe by generating a kind of Yukawa-like potential for gravitation [15]. The initial linear approach to massive gravity contained a Boulware-Deser ghost, which was cured in the dRGT version [16–19]. Massive gravity also features interesting properties for holography.

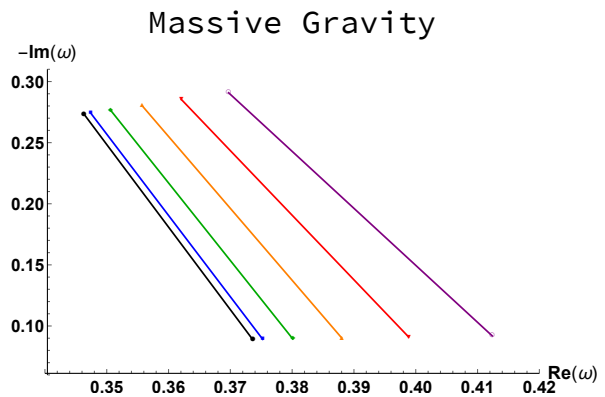


FIG. 1. QNMs for $l = 2$ in massive gravity. The dark points correspond to the Schwarzschild QNMs. The constants a , b and c have been fixed to one. From left to right: $m = \{15, 30, 45, 60, 75\} \times 10^{-3}$.

Starting from the action

$$S = \frac{1}{16\pi} \int d^4x \sqrt{-g} (R + m^2 \mathcal{U}(g, \phi^a)), \quad (32)$$

where R is the Ricci scalar and \mathcal{U} is the potential for the graviton, the following black hole solution can be derived [20, 21]:

$$f(r) = 1 - \frac{2M}{r} + \frac{\Lambda r^2}{3} + \gamma r + \epsilon, \quad (33)$$

where Λ , γ and ϵ are, respectively

$$\begin{aligned} \Lambda &= 3m^2(1 + a + b), \\ \gamma &= -cm^2(1 + 2a + 3b), \\ \epsilon &= c^2m^2(a + 3b), \end{aligned} \quad (34)$$

a and b being two dimensionless constant and c a positive constant with the dimension of a length. It should also be pointed out that a positive value of γ might also raise consistency issues [21].

The results are presented in Fig. 1 for $l = 2$. The values chosen for the constants do of course change the amplitude of the displacement of the QNMs. The global trend, which is the point of this study, however remains the same. Increasing of the graviton mass m tends to increase the real part of QNMs, that is the frequency of the oscillations. The difference in frequency between the fundamental and the first overtone also increases with m . The effect on the imaginary part is hardly noticeable on the plot even though a slight increase should be noticed, which is actually 50% less important, in relative variation, than the shift in frequency. The values considered here for the mass are, of course, way out of the known

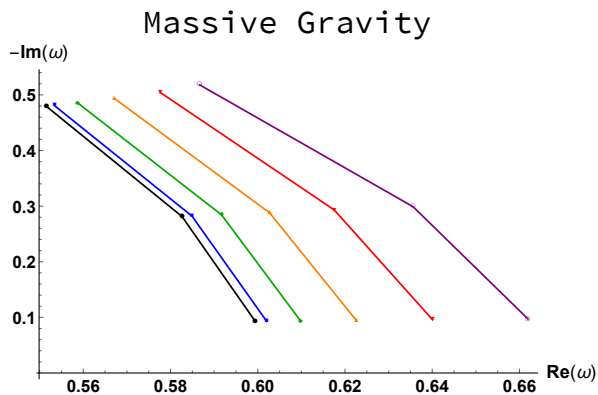


FIG. 2. QNMs for $l = 3$ in massive gravity. The dark points correspond to the Schwarzschild QNMs. The arbitrary constants a , b and c have been taken to one. From left to right: $m = \{15, 30, 45, 60, 75\} \times 10^{-3}$.

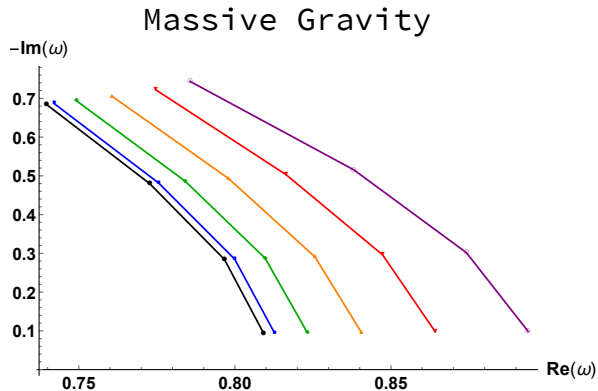


FIG. 3. QNMs for $l = 4$ in massive gravity. The dark points correspond to the Schwarzschild QNMs. The arbitrary constants a , b and c have been taken to one. From left to right: $m = \{15, 30, 45, 60, 75\} \times 10^{-3}$.

bounds but this is clearly not the point. Figures 2 and 3 show the results for $l = 3$ and $l = 4$. As a specific feature, one can notice that the frequency shift due to massive corrections decreases for higher overtones.

2. Modified STV gravity

The Scalar-Tensor-Vector modified gravitational theory (MOG) allows the gravitational constant, a vector field coupling and the vector field mass to vary with space and time [22]. The equations of motion lead to an effective modified acceleration law that can account for galaxy rotation curves and cluster observation without dark matter. Although it has recently been much debated and put under pressure, the theory is still worth being considered seriously. We consider the field equation

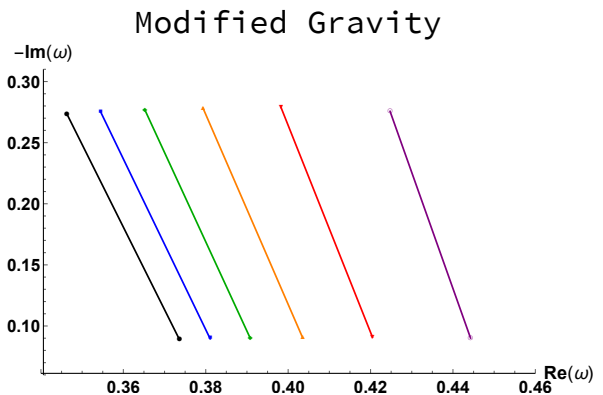


FIG. 4. QNMs for $l = 2$ in modified gravity. The dark points correspond to the Schwarzschild QNMs. From left to right: $\alpha = 1, 2, 3, 4, 5 \times 10^{-1}$.

for the metric tensor [23] :

$$R_{\mu\nu} = -8\pi G T_{\phi\mu\nu}, \quad (35)$$

where the gravitational coupling is $G = G_N(1+\alpha)$. With $B_{\mu\nu} = \partial_\mu\phi_\nu - \partial_\nu\phi_\mu$, the energy-momentum tensor for the vector field is :

$$T_{\phi\mu\nu} = -\frac{1}{4\pi}(B_\mu^\alpha B_{\nu\alpha} - \frac{1}{4}g_{\mu\nu}B^{\alpha\beta}B_{\alpha\beta}), \quad (36)$$

the constant ω of [22] being set to one. Solving the vacuum field equations

$$\nabla_\nu B^{\mu\nu} = \frac{1}{\sqrt{-g}}\partial_\nu(\sqrt{-g}B^{\mu\nu}) = 0, \quad (37)$$

and

$$\nabla_\sigma B_{\mu\nu} + \nabla_\mu B_{\nu\sigma} + \nabla_\nu B_{\sigma\mu} = 0, \quad (38)$$

with the appropriate symmetry leads to the metric

$$f(r) = 1 - \frac{2M}{r} + \frac{\alpha(1+\alpha)M^2}{r^2}. \quad (39)$$

We consider the relevant case $\alpha < \alpha_c = 0.67$ where there are two horizons and an appropriate potential behavior for the WKB approximation to hold.

The results are given in 4 for $l = 2$. The imaginary part of the QNMs is nearly the same whatever the value of α : the modified metric has no effect on the damping rate. However, increasing α does increase of the real part, that is the frequency. The effect is important for values near the critical value α_c . The slope is nearly independent of α . Figures 5 and 6 show the results for $l = 3$ and $l = 4$. The curves remain parallel on to the other: increasing the deformation parameter does not change the frequency shift between overtones.

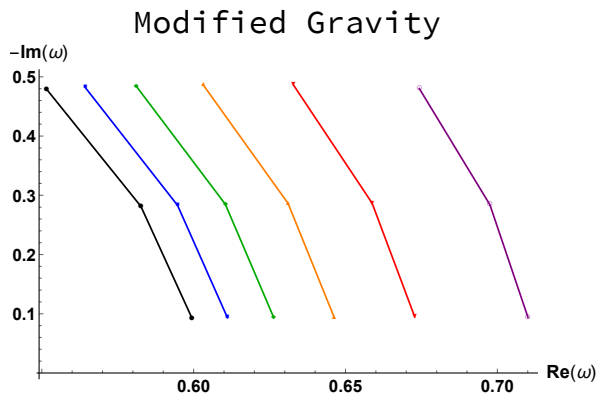


FIG. 5. QNMs for $l = 3$ in modified gravity. The dark points correspond to the Schwarzschild QNMs. From left to right: $\alpha = 1, 2, 3, 4, 5 \times 10^{-1}$.

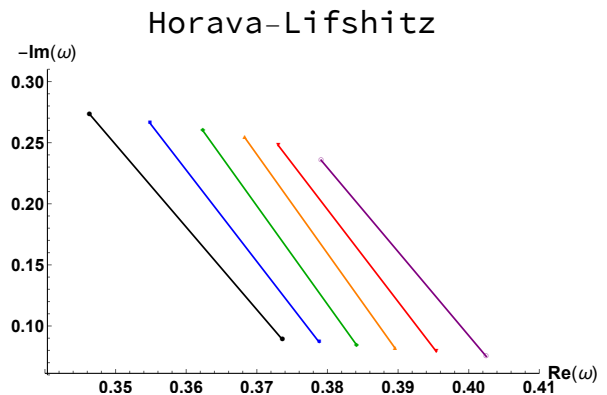


FIG. 7. QNMs for $l = 2$ in Horava-Lifshits gravity. The dark points correspond to the Schwarzschild QNMs. From left to right: $\beta = \{15, 30, 45, 60, 75\} \times 10^{-2}$.

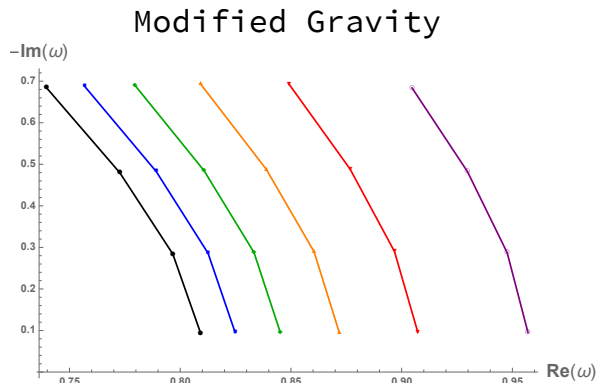


FIG. 6. QNMs for $l = 4$ in modified gravity. The dark points correspond to the Schwarzschild QNMs. From left to right: $\alpha = 1, 2, 3, 4, 5 \times 10^{-1}$.

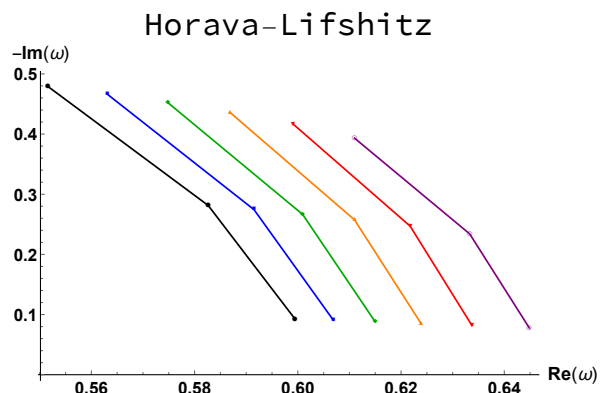


FIG. 8. QNMs for $l = 3$ in Horava-Lifshits gravity. The dark points correspond to the Schwarzschild QNMs. From left to right: $\beta = \{15, 30, 45, 60, 75\} \times 10^{-2}$.

3. Hořava-Lifshitz gravity

Hořava-Lifshitz gravity bets on the fundamental nature of the quantum theory instead of relying on GR principles. It is a renormalizable UV-complete gravitational theory which is not Lorentz invariant in $3 + 1$ dimensions [24]. The relativistic time with its Lorentz invariance emerges only at large distances. Black hole solutions have been found [25–27] and QNMs were studied [28].

Using the ansatz

$$ds^2 = -N^2(r) dt^2 + \frac{dr^2}{f(r)} + r^2(d\theta^2 + \sin^2\theta d\phi^2) \quad (40)$$

in the action, one is led to the Lagrangian

$$\begin{aligned} \tilde{\mathcal{L}}_1 = & \frac{\kappa^2 \mu^2 N}{8(1-3\lambda)\sqrt{f}} \left(\frac{\lambda-1}{2} f'^2 - \frac{2\lambda(f-1)}{r} f' \right) \\ & + \frac{(2\lambda-1)(f-1)^2}{r^2} - 2w(1-f-rf') \end{aligned} \quad (41)$$

where $w = 8\mu^2(3\lambda-1)/\kappa^2$. For $\lambda = 1$, the solution is

$$N^2 = f(r) = \frac{2(r^2 - 2Mr + \beta)}{r^2 + 2\beta + \sqrt{r^4 + 8\beta Mr}}, \quad (42)$$

with $\beta = 1/(2w)$, w being the deformation parameter entering the action given in [26]. There are two horizons for $M^2 > \beta$.

The results are given in Fig. 7. The frequency increases with an increase of β . Interestingly, the first overtone exhibits a quite high sensibility of its imaginary part: the damping rate varies substantially with β .

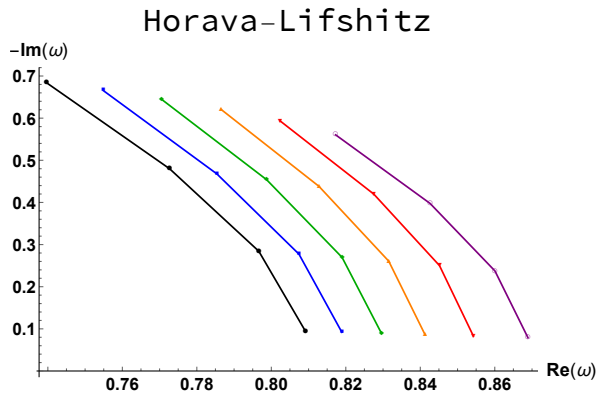


FIG. 9. QNMs for $l = 4$ in Horava-Lifshits gravity. The dark points correspond to the Schwarzschild QNMs. From left to right: $\beta = \{15, 30, 45, 60, 75\} \times 10^{-2}$.

Figures 8 and 9 give the results for $l = 3$ and $l = 4$ and it is worth noticing that the previously mentioned effect remains true for higher multipole momenta. The relative variation of the imaginary part is nearly the same whatever the overtone number.

4. \hbar correction

It has been known for a long time that quantum corrections to the Newtonian gravitational potential can be rigorously derived without having a full quantum theory of gravity at disposal (see, *e.g.*, [29–33] to cite only a few works from a very long list). Recently, a quite similar approach was developed [34] requiring that the quantum mechanically-corrected metric reproduces the corrected Newtonian limit, reproduces the standard result for the entropy of black holes including the known corrections, and fulfills some consistency conditions regarding the geodesic motion.

The resulting metrics reads as

$$f(r) = 1 - \frac{2M}{r} + \gamma \frac{2M}{r^3}. \quad (44)$$

We use here natural units but the last term is obviously proportional to \hbar . Interestingly, there is a long controversy about the value and the sign of the γ factor. From the phenomenological perspective, we do not fix it to a particular value but we keep it negative, in agreement with the latest expectations.

The results are given in Fig. 10. For large values of γ , the effects are noticeable on the frequency. It is remarkable that, from our analysis, the real part of the complex frequency is only decreased, which is not the case for the other considered models. The higher the

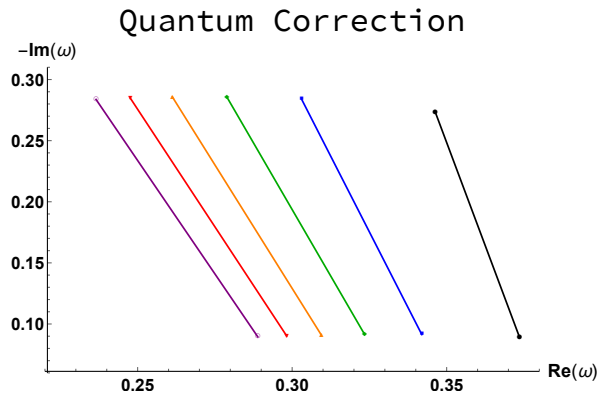


FIG. 10. QNMs for $l = 2$ in quantum-corrected gravity. The dark points correspond to the Schwarzschild QNMs. From left to right: $\gamma = -4.1, -3.3, -2.5, -1.8, -0.9$.

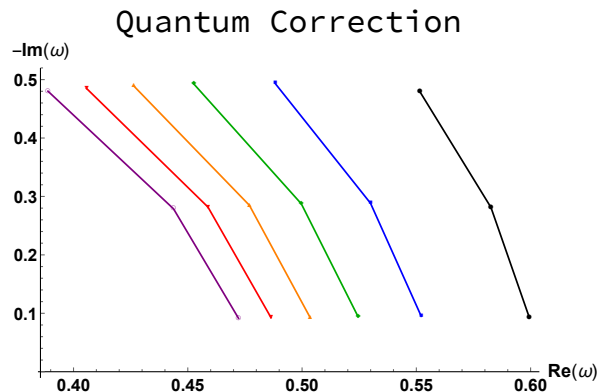


FIG. 11. QNMs for $l = 2$ in quantum-corrected gravity. The dark points correspond to the Schwarzschild QNMs. From left to right: $\gamma = -4.1, -3.3, -2.5, -1.8, -0.9$.

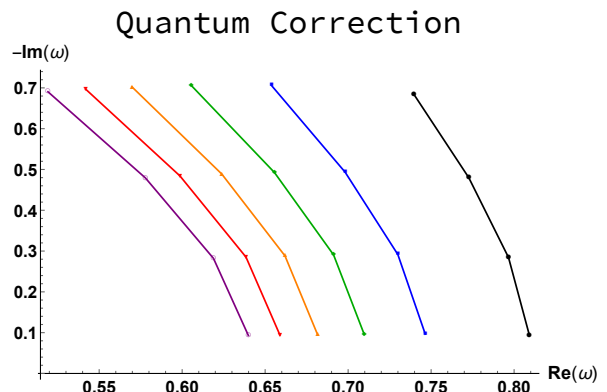


FIG. 12. QNMs for $l = 4$ in quantum-corrected gravity. The dark points correspond to the Schwarzschild QNMs. From left to right: $\gamma = -4.1, -3.3, -2.5, -1.8, -0.9$.

absolute value of γ , the larger the difference of frequency between the fundamental and the first overtone. Figures 11 and 12 show the results for $l = 3$ and $l = 4$.

5. LQG polymeric BH

Loop Quantum Gravity (LQG) is non-perturbative and background-invariant quantum theory of gravity [35]. In the covariant formulation, space is described by a spin network [36]. Each edge carries a “quantum of area”, labelled by a half integer j , associated with an irreducible representations of $SU(2)$. Each node carries a “quantum of space” associated with an intertwiner. A key result is that area is quantized according to

$$A(j) = 8\pi\gamma_{BI}\sqrt{j(j+1)}, \quad (45)$$

with γ_{BI} the Barbero-Immirzi parameter. Black holes are usually described in LQG through an isolated horizon puncturing a spin network [37] and the phenomenology is very rich, depending on the precise setting chosen [38]. We focus here on the model developed in [39] where a regular lattice with edges of lengths δ_b and δ_c is considered. Requiring the minimal area to be one derived in LQG, one is left with only one free parameter δ . From this minisuperspace approximation, a static spherical solution can be derived and is given by

$$\begin{aligned} ds^2 &= -G(r)dt^2 + \frac{dr^2}{F(r)} + H(r)d\Omega^2, \\ G(r) &= \frac{(r-r_+)(r-r_-)(r+r_*)^2}{r^4 + a_0^2}, \\ F(r) &= \frac{(r-r_+)(r-r_-)r^4}{(r+r_*)^2(r^4 + a_0^2)}, \\ H(r) &= r^2 + \frac{a_0^2}{r^2}, \end{aligned} \quad (46)$$

where $d\Omega^2 = d\theta^2 + \sin^2\theta d\phi^2$, $r_+ = 2m$ and $r_- = 2mP^2$ are the two horizons, and $r_* = \sqrt{r_+r_-} = 2mP$, P being the polymeric function defined by $P = (\sqrt{1+\epsilon^2} - 1)/(\sqrt{1+\epsilon^2} + 1)$, with $\epsilon = \gamma_{BI}\delta$, and the area parameter a_0 is given by $a_0 = A_{min}/8\pi$. The parameter m in the solution is related to the ADM mass M by $M = m(1+P)^2$.

The results are given in Fig. 13. The damping rate does not depend at all upon the polymerization parameter. The real part of the complex frequency does, however, increase with δ . Noticeably, the slope is unchanged and varying the deformation parameter just lead to a horizontal translation of the QNM frequency in the complex plane. This means that the frequency shift between the fundamental and the overtones does not depend on

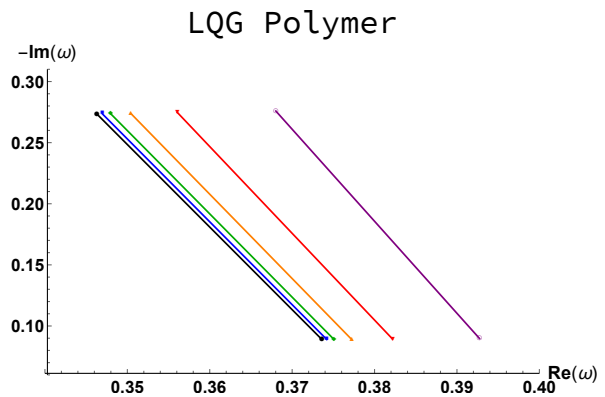


FIG. 13. QNMs for $l = 2$ in LQG (polymer BHs). The dark points correspond to the Schwarzschild QNMs. The parameters are $a_0 = 1$ and from left to right: $\epsilon = 10^{-1}, -0.8, -0.6, -0.4, -0.2$.

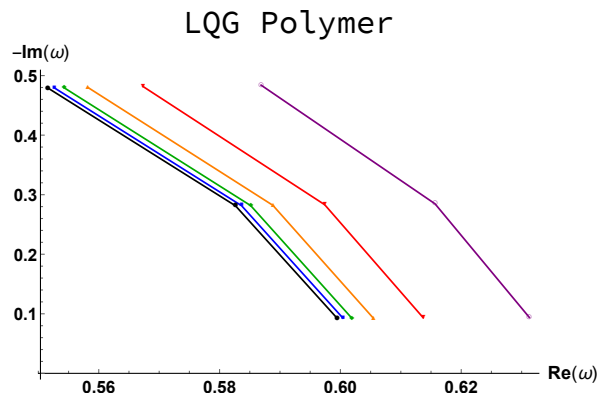


FIG. 14. QNMs for $l = 2$ in LQG (polymer BHs). The dark points correspond to the Schwarzschild QNMs. The parameters are $a_0 = 1$ and from left to right: $\epsilon = 10^{-1}, -0.8, -0.6, -0.4, -0.2$.

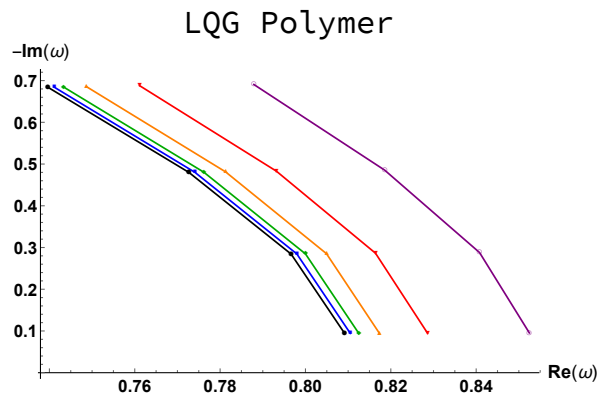


FIG. 15. QNMs for $l = 4$ in LQG (polymer BHs). The dark points correspond to the Schwarzschild QNMs. The parameters are $a_0 = 1$ and from left to right: $\epsilon = 10^{-1}, -0.8, -0.6, -0.4, -0.2$.

the amplitude of the quantum gravity corrections, as in modified gravity. Figures 14 and 15 give the results for $l = 3$ and $l = 4$.

CONCLUSION

This study shows the evolution of the complex frequency of quasinormal modes of a Schwarzschild black holes for the fundamental, the first overtones and a few multipole numbers. We have considered massive gravity, STV gravity, Hořava-Lifshitz gravity, quantum corrected gravity, and loop quantum gravity. All the results were derived using the very same WKB approximation scheme which makes a meaningful comparison possible.

Obviously, distinguishing between those models with observations is more than challenging. First, because there exist degeneracies, for given overtone and multipole numbers, between the models – when taking into account that the values of the parameters controlling the deformation are unknown. Second, because the intrinsic characteristics of the observed black holes are also unknown, which induces other degeneracies. In addition, this study should be extended to Kerr black hole, which also adds some degeneracies in addition to the complexity.

Some interesting trends can however be underlined. For all models, the effect of modifying the gravitational theory are more important for the real part than for the imaginary part of the complex frequency of the QNMs. Otherwise stated, the frequency shift is more important than the change in the damping rate. In addition, the sign of the frequency shift, and its dependence upon the overtone and multipole numbers is characteristic of a given model. The accurate patterns are never the same, which is an excellent point for phenomenology. It can basically be concluded that a meaningful use of QNMs to investigate efficiently modified gravity requires the measurement of several relaxation modes. This is in principle possible but way beyond the sensitivity of current interferometers. The goal of this study was not to perform a detailed analysis of the discrimination capabilities of gravitational wave experiments: it simply aimed at exhibiting the main tendencies for fashionable extended gravity models, as an introduction to this special issue on “probing new physics with black holes”.

[1] C. Chirenti, *Braz. J. Phys.* **48**, 102 (2018), 1708.04476.
 [2] S. Chandrasekhar, in *Oxford, UK: Clarendon (1992) 646 p.*, OXFORD, UK: CLARENDON (1985) 646 P. (1985).
 [3] F. Moulin and A. Barrau (2019), 1906.05633.

[4] K. D. Kokkotas and B. G. Schmidt, *Living Rev. Rel.* **2**, 2 (1999), gr-qc/9909058.
 [5] H.-P. Nollert, *Class. Quant. Grav.* **16**, R159 (1999).
 [6] E. Berti, V. Cardoso, and S. Yoshida, *Phys. Rev.* **D69**, 124018 (2004), gr-qc/0401052.
 [7] E. N. Dorband, E. Berti, P. Diener, E. Schnetter, and M. Tiglio, *Phys. Rev.* **D74**, 084028 (2006), gr-qc/0608091.
 [8] R. A. Konoplya, *Phys. Rev.* **D68**, 024018 (2003), gr-qc/0303052.
 [9] B. Mashhoon, in *3rd Marcel Grossmann Meeting on the Recent Developments of General Relativity Shanghai, China, August 30-September 2, 1982* (1982), pp. 599–608.
 [10] B. F. Schutz and C. M. Will, *Astrophys. J.* **291**, L33 (1985).
 [11] S. Iyer and C. M. Will, *Phys. Rev.* **D35**, 3621 (1987).
 [12] S. Iyer, *Phys. Rev.* **D35**, 3632 (1987).
 [13] K. D. Kokkotas and B. F. Schutz, *Phys. Rev.* **D37**, 3378 (1988).
 [14] R. A. Konoplya, A. Zhidenko, and A. F. Zinhailo (2019), 1904.10333.
 [15] G. D’Amico, C. de Rham, S. Dubovsky, G. Gabadadze, D. Pirtskhalava, and A. J. Tolley, *Phys. Rev.* **D84**, 124046 (2011), 1108.5231.
 [16] C. de Rham and G. Gabadadze, *Phys. Rev.* **D82**, 044020 (2010), 1007.0443.
 [17] C. de Rham, G. Gabadadze, and A. J. Tolley, *Phys. Rev. Lett.* **106**, 231101 (2011), 1011.1232.
 [18] S. F. Hassan and R. A. Rosen, *JHEP* **07**, 009 (2011), 1103.6055.
 [19] C. de Rham, *Living Rev. Rel.* **17**, 7 (2014), 1401.4173.
 [20] S. G. Ghosh, L. Tanmukij, and P. Wongjun, *Eur. Phys. J.* **C76**, 119 (2016), 1506.07119.
 [21] B. Eslam Panah, S. H. Hendi, and Y. C. Ong (2018), 1808.07829.
 [22] J. W. Moffat, *JCAP* **0603**, 004 (2006), gr-qc/0506021.
 [23] J. W. Moffat, *Eur. Phys. J.* **C75**, 175 (2015), 1412.5424.
 [24] P. Horava, *Phys. Rev.* **D79**, 084008 (2009), 0901.3775.
 [25] E. O Colgain and H. Yavartanoo, *JHEP* **08**, 021 (2009), 0904.4357.
 [26] A. Kehagias and K. Sfetsos, *Phys. Lett.* **B678**, 123 (2009), 0905.0477.
 [27] H. Lu, J. Mei, and C. N. Pope, *Nucl. Phys.* **B806**, 436 (2009), 0804.1152.
 [28] S. Chen and J. Jing, *Phys. Lett.* **B687**, 124 (2010), 0905.1409.
 [29] J. F. Donoghue, *Phys. Rev. Lett.* **72**, 2996 (1994), gr-qc/9310024.
 [30] J. F. Donoghue, *Phys. Rev.* **D50**, 3874 (1994), gr-qc/9405057.
 [31] N. E. J. Bjerrum-Bohr, J. F. Donoghue, and B. R. Holstein, *Phys. Rev.* **D68**, 084005 (2003), [Erratum: *Phys. Rev.* **D71**, 069904(2005)], hep-th/0211071.
 [32] N. E. J. Bjerrum-Bohr, J. F. Donoghue, and B. R. Holstein, *Phys. Rev.* **D67**, 084033 (2003), [Erratum: *Phys. Rev.* **D71**, 069903(2005)], hep-th/0211072.
 [33] N. E. J. Bjerrum-Bohr, J. F. Donoghue, B. R. Holstein, L. Plant, and P. Vanhove, *Phys. Rev. Lett.* **114**, 061301 (2015), 1410.7590.
 [34] P. Bargueo, S. Bravo Medina, M. Nowakowski, and D. Batic, *EPL* **117**, 60006 (2017), 1605.06463.
 [35] A. Ashtekar, *Lect. Notes Phys.* **863**, 31 (2013), 1201.4598.

- [36] C. Rovelli, PoS **QGQS2011**, 003 (2011), 1102.3660.
- [37] A. Perez, Rept. Prog. Phys. **80**, 126901 (2017), 1703.09149.
- [38] A. Barrau, K. Martineau, and F. Moulin, Universe **4**, 102 (2018), 1808.08857.
- [39] E. Alesci and L. Modesto, J. Phys. Conf. Ser. **360**, 012036 (2012).